

The “Pacemaker of the Ice Ages” Paper Revisited: Closing a Loophole in the Refutation of a Key Argument for Milankovitch Climate Forcing

Jake Hebert*

Abstract

The 1976 “Pacemaker of the Ice Ages” paper by Hays, Imbrie, and Shackleton largely convinced the secular scientific community that Earth’s orbital and rotational motions are affecting climate. The authors performed power spectrum analyses on variables of presumed climatic significance within two deep-sea Indian Ocean sediment cores, analyses that showed dominant spectral peaks at frequencies corresponding to calculated 100-, 41-, and 23-thousand-year astronomical cycles. Previous research showed serious problems with this paper, as it implicitly assumed an age of 700 thousand years for the Brunhes-Matuyama (B-M) magnetic reversal boundary, rather than the currently-accepted age of 780 thousand years. Furthermore, secular scientists have argued for the existence of discontinuities in the cores that were used either directly or indirectly in the analyses, and they have also made modifications to the data sets used in the Pacemaker analysis. When all these changes are taken into account, the Pacemaker analysis provides no convincing support for the currently-accepted version of the Milankovitch hypothesis. In fact, agreement with Milankovitch expectations is worse than the previously published new results obtained using the reconstructed original data sets.

Introduction

The astronomical (or Milankovitch) hypothesis is the currently dominant secular explanation for the fifty or so Pleistocene ice ages said to have occurred within the last 2.6 million years (Walker and Lowe, 2007). Although the theory has many seri-

ous problems (Oard, 2005, 2007, 2014; Cronin, 2010), it is now widely accepted on the basis of a 1976 paper published in *Science* entitled “Variations in the Earth’s Orbit: Pacemaker of the Ice Ages” (Hays, Imbrie, and Shackleton, 1976). Because the astronomical hypothesis of climate forcing implicitly assumes

* Jake Hebert, Institute for Creation Research, Dallas, TX, contact@icr.org

Accepted for Publication January 17, 2018

the existence of “deep time,” the Pacemaker paper has become not just a key argument for the astronomical hypothesis, but an iconic argument for an old Earth as well. The significance of the Pacemaker paper is indicated by the fact that both *Nature* and *Science* published articles commemorating its fortieth anniversary (Maslin, 2016; Hodell, 2016).

Hays, Imbrie, and Shackleton performed spectral analyses on three variables within two southern Indian Ocean deep-sea sediment cores designated as RC11–120 and E49–18. These three variables were the oxygen isotope ratios (denoted by the shorthand notation $\delta^{18}\text{O}$) of the foraminiferal species *Globigerina bulloides*, the percent abundance of the radiolarian species *Cyclodophora davisiana*, and (southern hemisphere) summer sea surface temperatures, also inferred from radiolarian data. The results showed climate cycles corresponding to periods of 100, 42, and 23 thousand years (100, 42, and 23 ka). They also showed evidence of a 19 ka cycle, although others (Muller and MacDonald, 2000, pp. 74–78) have argued that this apparent cycle was not “real.” Since orbital calculations show dominant cycles having nearly those same lengths (100, 41, and 23 thousand years), the Pacemaker paper was seen as strong evidence for the hypothesis of Milankovitch climate forcing.

However, the original Pacemaker results are invalid (Hebert, 2016c), even by uniformitarian reckoning, due to a significant age revision made by uniformitarian scientists in the early 1990s. In order to better understand the methodology of the Pacemaker paper and why its results are invalid, it is necessary to first cover some background material. Readers already familiar with the concepts of oxygen isotope ratios and Marine Isotope Stages (MIS) may wish to skip the following two sections.

Background: Foraminiferal Oxygen Isotope Values

Microscopic marine creatures called foraminifera construct shells, or tests, that are composed of calcium carbonate (CaCO_3). Planktonic foraminifera float freely in the water column (Mortyn and Charles, 2003), whereas benthic foraminifera live on or in the seafloor sediments (Kingston, 2010). When these organisms die, their shells contribute to the debris accumulating on the ocean floor. Scientists often measure the ^{18}O and ^{16}O isotopes in a foraminiferal shell and use this to calculate a quantity called the oxygen isotope ratio, indicated by the symbol $\delta^{18}\text{O}$. These values are reported relative to a standard $\delta^{18}\text{O}$ value, in units of parts per thousand (“per mille,” or ‰):

$$\delta^{18}\text{O} = \frac{\left(\frac{^{18}\text{O}}{^{16}\text{O}}\right)_{\text{sample}} - \left(\frac{^{18}\text{O}}{^{16}\text{O}}\right)_{\text{standard}}}{\left(\frac{^{18}\text{O}}{^{16}\text{O}}\right)_{\text{standard}}} \times 1000 \text{‰} \quad (1)$$

Evaporation preferentially favors the removal of ‘lighter’ isotopes (such as ^{16}O) from a reservoir of oxygen atoms (such as water molecules in an ocean), and this preferential evaporation is more pronounced at lower temperatures. Hence, during an ice age, one would expect the oceans to be more depleted in ^{16}O , or equivalently, more enriched in ^{18}O , compared to some standard value. Since foraminifera use oxygen atoms to make their shells, one thus expects higher $\delta^{18}\text{O}$ values in shells constructed by foraminifera during an ice age. Therefore, the oxygen isotope signal within a sediment core is thought to be a climate indicator, with higher $\delta^{18}\text{O}$ values indicating colder temperatures or, more precisely, times of high global ice volume (Wright, 2010). Likewise, lower $\delta^{18}\text{O}$ values within the sediments are thought to indicate times of low global ice volume. Conversely, higher (less negative) $\delta^{18}\text{O}$ values within ice cores are thought to correspond to times of less global ice volume, and lower (or more negative) $\delta^{18}\text{O}$ values are thought to correspond to times of greater global ice volume. Of course, creation scientists have long pointed out issues that complicate this simplistic understanding of seafloor sediment and ice core $\delta^{18}\text{O}$ values (Oard, 1984; Vardiman, 1997).

Nevertheless, the Pacemaker authors used planktonic oxygen isotope ratios from the two Indian Ocean sediment cores in their analysis (Hays, Imbrie, and Shackleton, 1976). This is potentially problematic, since planktonic $\delta^{18}\text{O}$ values are much more susceptible to short-term, local temperature and chemical variations than benthic $\delta^{18}\text{O}$ values (Oard, 1984; Karner et al., 2002, p. 1). Hence, it may not represent a truly global climate signal, even within a uniformitarian framework. However, we here overlook this potential difficulty and focus on other problems with the Pacemaker paper.

Background: Marine Isotope Stages

Because uniformitarian scientists believe that this oxygen isotope signal is a global climate indicator (Prell et al., 1986, p. 137), they believe that, in theory, the oxygen isotope signal, plotted as a function of depth, for one sediment core should look basically the same as the oxygen isotope signal for another sediment core. Of course, uniformitarians recognized that in actual practice this will rarely be the case; changes in sedimentation rates, local weather effects, post-depositional processes, etc., can obscure or distort this idealized signal. Nevertheless, if oxygen isotope features can somehow be accurately dated in one sediment core, uniformitarian scientists believe that it should be possible to transfer those ages to (presumed) corresponding oxygen isotope features in another sediment core (Figure 1).

In order to facilitate this “wobble matching” process, uniformitarian scientists devised a concept called marine

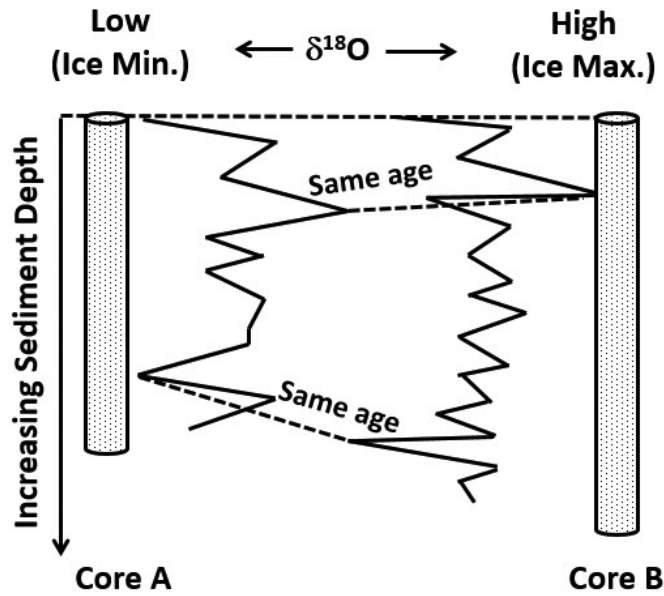


Figure 1. Because uniformitarian scientists believe that the oxygen isotope ($\delta^{18}\text{O}$) signal is a global climate indicator, they assume that similar $\delta^{18}\text{O}$ features in different sediment cores are the same age (provided that the $\delta^{18}\text{O}$ signals in the cores have not been distorted by local weather effects, post-depositional processes, etc.).

isotope stages (MIS). Generally, but with some exceptions, odd-numbered marine isotope stages indicate warm periods (interglacials), and even-numbered marine isotope stages denote ice ages (glacials). The boundaries between marine isotope stages are generally located at depths at which the $\delta^{18}\text{O}$ signal has transitioned halfway from a local minimum to a local maximum, or *vice versa* (Gibbard, 2007). Prominent features within a particular marine isotope stage are indicated with a number following a decimal. Particularly low $\delta^{18}\text{O}$ values within a marine isotope stage (indicating times of relative warmth within a glacial or interglacial) are indicated by odd numbers after the decimal, whereas particularly high $\delta^{18}\text{O}$ values within the MIS (indicating times of relative coolness in a glacial or interglacial) are indicated by even numbers after the decimal, with the post-decimal numbers decreasing as one moves up the core toward younger ages. For instance, MIS 5 is thought to contain three dominant $\delta^{18}\text{O}$ troughs, labelled as 5.1, 5.3, and 5.5, with 5.1 being the youngest and 5.5 being the oldest. Originally, the entirety of MIS 5 was thought to be an interglacial, but now uniformitarian scientists argue that this is only true of MIS 5.5. MIS events 5.1 and 5.3 have since been grouped together with MIS 2, 3, and 4 and counted as

representing the most recent ice age (McManus et al., 1994, p. 326). By convention, MIS boundaries between two marine isotope stages are indicated by the number of the earlier stage followed by a decimal and a zero. For instance, the boundary between stages 1 and 2 is denoted as MIS 2.0

Age Assignments for the Pacemaker Paper

Prior to performing their analyses, the Pacemaker authors had to assign tentative timescales to the two Indian Ocean cores. Even uniformitarians acknowledge that, with some exceptions (e.g., radiocarbon dating of the uppermost sediments and uranium series dating), radioisotope dating methods cannot be used to directly date seafloor sediments. Hence, they had to use a “backdoor” approach to obtain these preliminary age-scales. Potassium-argon dating had previously been used to assign an age of 700 ka to volcanic rocks recording what was believed to be the most recent “flip” or “reversal” of the earth’s magnetic field, the Brunhes-Matuyama (B-M) magnetic reversal (Shackleton and Opdyke, 1973).

Uniformitarians believe that magnetic reversals occur slowly, taking on average about seven thousand years, although with a large degree of latitude-dependent variation (Clement, 2004). However, uniformitarian scientists themselves have claimed evidence for multiple, extremely rapid, past magnetic reversal events (Coe, Prévot, and Camps, 1995; Bogue and Glen, 2010; Sagnotti et al., 2014). Hence, the evidence would seem to strongly favor rapid magnetic reversals, which are quite unexpected in the uniformitarian framework. Creation scientists associate these reversals with the upheaval of the Genesis Flood and argue that the apparent erratic timing of the reversals is a consequence of an incorrect uniformitarian timescale (Humphreys, 1986, 1990).

Since seafloor sediments contain magnetic minerals, they can, in principle, also record these magnetic reversals. Therefore, uniformitarians transferred this age of 700 ka to the most recent apparent magnetic reversal (located at a depth of 1200 cm) within the western Pacific core V28–238 (Hays, Imbrie, and Shackleton, 1976; Shackleton and Opdyke, 1973). The V28–238 core is extremely important to uniformitarian scientists because of the (presumed) very constant rate at which its sediments were deposited; its deposition rate was thought to be the most constant of any deep-sea cores then in existence (Shackleton, Berger, and Peltier, 1990, p. 258). Hence, if the age of the top of the V28–238 core were known, uniformitarian scientists could then use the assumption of a constant sedimentation rate to assign ages to the marine isotope stage boundaries within the V28–238 core, and, since the isotopic signal was assumed to be globally synchronous, these ages could then be transferred to the oxygen isotope signals in *other* sediment cores. Because of its importance, the isotope

record in the V28–238 core has been called a kind of ice age “Rosetta Stone” (Woodward, 2014, p. 97). The Pacemaker authors transferred some of these MIS boundary ages to the (presumably) corresponding isotopic features in the RC11–120 and E49–18 Indian Ocean cores.

However, in the early 1990s, uniformitarian scientists arbitrarily raised the age of the B-M magnetic reversal boundary to 780 ka (Shackleton, Berger, and Peltier, 1990; Hilgen, 1991) so that isotopic wiggles in *other* sediment cores would agree with Milankovitch expectations! This revision was later ostensibly “confirmed” by radioisotope dating (Spell and McDougall, 1992). However, uniformitarians never went back to see what this age revision would do to the original Pacemaker results. Hebert (2016c) used Shackleton and Opdyke’s (1973) method to recalculate the ages for the marine isotope stage boundaries using this new age assignment and then re-performed the Pacemaker calculations. The results showed that this age revision significantly weakened the case for Milankovitch climate forcing.

In fact, there is a “shortcut” by which even non-specialists can quickly verify that these new results are at least approximately correct (Hebert, 2017a, c, d), using nothing more than a pocket calculator and basic high school algebra. Furthermore, there are good reasons to suspect that uniformitarian scientists do not have a good “replacement” for the Pacemaker paper (Hebert, 2017b), which means that there is no objective evidence for the astronomical theory (hypothesis, really), even within a uniformitarian framework.

Revised Data Values

However, uniformitarians have made other changes that conceivably could also have affected the results of the Pacemaker analysis. For the sake of rigor, these additional changes should also be taken into account when redoing the calculations.

First, uniformitarians have made additional measurements within the RC11–120 and E49–18 cores, and these newer measurements sometimes disagree somewhat with the older measurements. For this analysis I used the most recent publicly available versions of the relevant data sets I could find. For the RC11–120 $\delta^{18}\text{O}$ values, I used the data of McIntyre and Imbrie (2000), accessed at <https://doi.pangaea.de/10.1594/PANGAEA.56357?format=html#download>. These data are shown in Figure 2.

For the E49–18 $\delta^{18}\text{O}$ data, I merged the 10 cm resolution data from Hays, Imbrie, and Shackleton (1997) with Rickaby and Elderfield’s (1999) higher resolution (5 cm) data for the uppermost core section. These data sets were accessed at <https://doi.pangaea.de/10.1594/PANGAEA.52207> and ftp://ftp.ncdc.noaa.gov/pub/data/paleo/paleocean/sediment_files/complete/e49-18r-tab.txt.

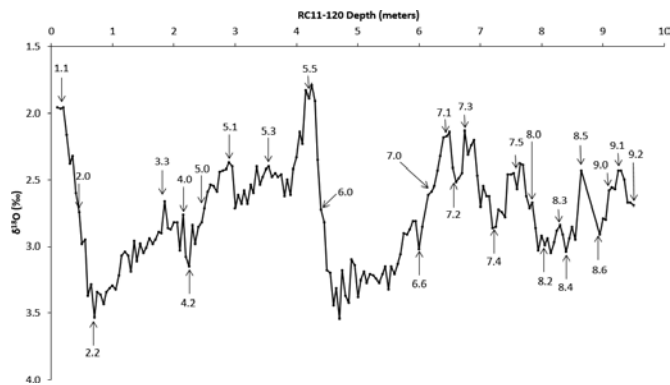


Figure 2. RC11–120 $\delta^{18}\text{O}$ values and MIS events.

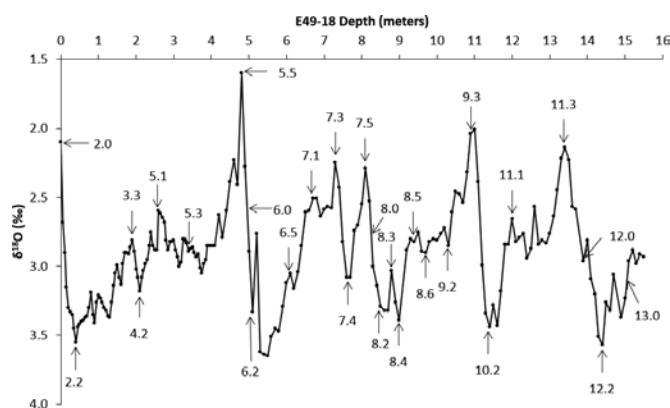


Figure 3. E49–18 $\delta^{18}\text{O}$ values and MIS events.

Actually, the values reported by Hays, Imbrie, and Shackleton (1997) in the upper core section were themselves the simple averages of the values reported by Rickaby and Elderfield (1999). Hays, Imbrie, and Shackleton reported two different $\delta^{18}\text{O}$ values (2.99‰ and 2.86‰) at a depth of 15.5 meters, so I used the simple average (2.93‰) of these two values at that depth. These data are shown in Figure 3.

Likewise, I used the RC11–120 SST values provided by Hays, Imbrie, and Shackleton (1997), which were archived at <https://doi.pangaea.de/10.1594/PANGAEA.52223?format=html#download>. SST values for the E49–19 core were provided by Howard and Prell (1992) and accessed at https://www1.ncdc.noaa.gov/pub/data/paleo/paleocean/sediment_files/sst/e49-18_ssts-tab.txt. Unlike the previous SST estimates, these new E49–18 SST estimates were based on foraminiferal, rather than radiolarian, data. However, the new SST estimates were generally “in phase” with the previous temperature estimates (Hebert, 2016a).

The SPECMAP values of the percentages of *C. davisiana* values within the RC11–120 core were provided by Martinson et al. (1987), and these were accessed at <https://doi.pangaea.de/10.1594/PANGAEA.51706?format=html>. For the percentages of *C. davisiana* within the E49–18 core, I used my values, which I reconstructed from Figures 2 and 3 in the Pacemaker paper (Hebert, 2016a, Table A6), as I could not find a compilation of these values elsewhere.

Alleged Core Discontinuities

Uniformitarians originally claimed that continuity of the V28–238 core was “virtually proved” (Emiliani and Shackleton, 1974, p. 513). However, they later reversed themselves and claimed that V28–238 had been disturbed within marine isotope stages 5 and 11 (Imbrie et al., 1984; Prell et al., 1986). However, the supposed discontinuity in stage 5 was not considered significant, as Prell et al. (1986, p. 149) did not attempt to correct for it. However, they did correct for supposed stretching of the core in stage 11; in order to compensate for this, three “extraneous” data points were removed (Prell et al., 1986, p. 149), causing depths below 723 cm in V28–238 to be decreased by 30 cm (Imbrie et al., 1984, p. 288). In some cases, uniformitarians revised these depth estimates slightly. See online V28–238 data archived at <https://doi.pangaea.de/10.1594/PANGAEA.51710?format=html#download>, which I used to construct my Figure 4. I also used these data, along with the data from Prell et al. (1986, pp. 144–148), to construct my Table 1. All MIS events in Table 1 came from Prell et al. (1986), with the exception of MIS events 13.0 and 13.1. Although Prell et al. (1986, p. 146) claimed that the MIS 13.0 boundary was “difficult to pick,” my identification of a depth of 781 cm with this boundary seems reasonable, given that Prell et al. identified the positive $\delta^{18}O$ peak to the right as MIS 13.2 and the $\delta^{18}O$ trough to the right of 13.2 as 13.3. Given those two choices, it seems obvious that the $\delta^{18}O$ trough to the left of MIS 13.2 (at a depth of 802 cm) should be MIS 13.1. And if that is the case, what else can the depth of 781 cm be but MIS 13.0?

These depth revisions alter the apparent depths of many of the MIS boundaries in V28–238. Likewise, the apparent depth of the B-M magnetic reversal boundary is revised to 1200 cm – 30 cm = 1170 cm (Prell et al., 1986, p. 148). Naturally, these revisions will alter the presumed ages for those MIS boundaries. Figure 5 illustrates Shackleton and Opdyke’s (1973) method for obtaining the ages for the MIS boundaries but uses new depth values and the revised age for the B-M reversal boundary. As noted earlier, Figure 4 depicts the V28–238 $\delta^{18}O$ signal plotted as a function of these adjusted depth values.

Of course, one should consider the possibility that there might also be hitherto unnoticed discontinuities in the

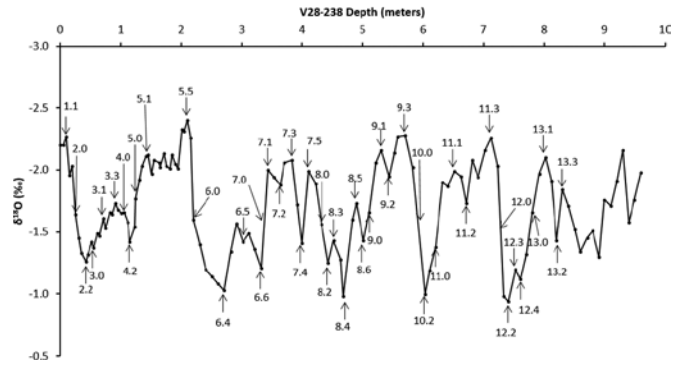


Figure 4. V28–238 $\delta^{18}O$ values as a function of revised depth values, with indicated marine isotope stage (MIS) events.

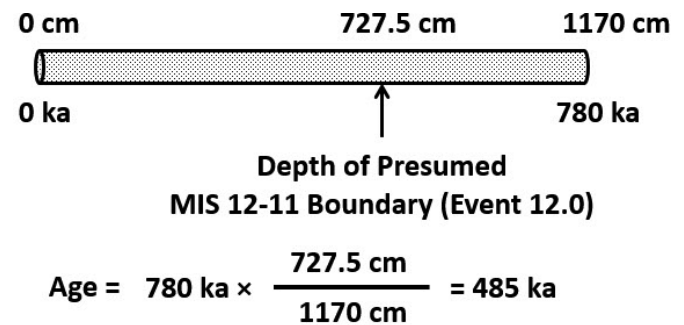


Figure 5. Demonstration of the method used by Shackleton and Opdyke (1973) to assign ages to the V28–238 marine isotope stage (MIS) boundaries, but using the revised age of the Brunhes-Matuyama magnetic reversal boundary and revised depths for the V28–238 data. Hays, Imbrie, and Shackleton used a handful of these (unadjusted) ages in their famous 1976 “Pacemaker of the Ice Ages” paper.

RC11–120 and E49–18 cores as well. This is addressed in the following sections.

Checking For Discontinuities in RC11–120 and E49–18: Shaw Diagrams

Correcting for these supposed discontinuities within the V28–238 sediment core should theoretically yield a plot of $\delta^{18}O$ versus depth that suffers from no remaining distortions. In that case, the assumed age of 0 ka at the core top would imply that the

Table 1. Depths of marine isotope stage events (up to 13.3) in the V28–238 deep-sea core, after accounting for the revisions described by Imbrie et al. (1984) and Prell et al. (1986).

MIS Event	V28–238 Min. Depth (cm)	V28–238 Most Likely Depth (cm)	V28–238 Max. Depth (cm)
1.1	5	10	15
2.0	15	25	30
2.2	35	42	45
3.0	45	55	65
3.1	62	71	75
3.3	85	91	101
4.0	101	105	115
4.2	111	115	123
5.0	123	125	135
5.1	135	145	151
5.5	201	210	215
6.0	215	220	251
6.4	261	271	282
6.5	282	302	322
6.6	322	332	343
7.0	332	337.5	343
7.1	332	343	353
7.2	353	364	370
7.3	364	383	392
7.4	392	399	410
7.5	399	410	432
8.0	422	432	443
8.2	432	443	452

MIS Event	V28–238 Min. Depth (cm)	V28–238 Most Likely Depth (cm)	V28–238 Max. Depth (cm)
8.3	443	452	463
8.4	463	468	483
8.5	483	489	501
8.6	489	501	511
9.0	501	511	522
9.1	522	531	543
9.2	531	543	552
9.3	552	571	583
10.0	583	593	603
10.2	595	603	611
11.0	611	620	641
11.1	632	652	663
11.2	663	671	691
11.3	691	712	722
12.0	722	727.5	733
12.2	733	741	752
12.3	741	752	761
12.4	752	761	771
13.0	741	781	792
13.1	781	802	821
13.2	812	821	830
13.3	821	830	840

revised depths within the V28–238 core are truly proportional to age. Hence, the (presumed correct) V28–238 $\delta^{18}\text{O}$ signal in Figure 2 can be used to test for disturbances and/or changes in sedimentation rates within *other* sediment cores. If one plots the depths at which particular $\delta^{18}\text{O}$ features were found within the V28–238 core on one axis of a graph, and the depths at which those same (presumed) features were found within another core on the other axis, the result is known as a Shaw diagram (Shaw, 1964; Prell et al., 1986). These plots often consist of a number of straight line segments, sometimes separated by “gaps” and/

or exhibiting discontinuities in their respective slopes. Together these line segments make up the “line of correlation” (LOC). Since the depths (from the V28–238 core) on the vertical axis are assumed to be correct, the depths on the horizontal axis may be “corrected” by mapping them onto the vertical axis, thereby converting them to the V28–238 “reference” depth scale. Once this has been done, the (presumed correct) V28–238 linear age scale is applied to the data from the test core.

Figure 6 illustrates the basic concept. A set of clearly identifiable MIS events common to both the reference core and the

test core is used to compare relative sedimentation rates in the two cores. Because there is some uncertainty in the depth of an MIS event, the events are represented by small rectangles, with the horizontal sides of the boxes indicating depth uncertainties in the test core and the vertical sides representing depth uncertainties in the reference core. These events are used to construct the line of correlation (LOC), with the LOC preferably passing through all the event boxes.

If one grants the assumptions that the $\delta^{18}\text{O}$ signal is globally synchronous *and* that the MIS events have been correctly identified in *both* cores, then the Shaw diagram can be used to compare relative sedimentation rates between the two cores. For instance, the time between events #1 and #2 in Figure 4 is Δt_1 in both cores, but during that time interval, a greater thickness of sediment was deposited in the reference core than in the test core, indicating that the sedimentation rate within the reference core was faster. However, during the time interval Δt_2 , a greater amount of sediment was deposited in the test core than in the reference core, indicating that for that time interval, the test core had a faster sedimentation rate.

Hence, changes in the slope of the line of correlation indicate a change in relative sedimentation rate between the two cores. Since the sedimentation rate of the reference core (in this case, the V28–238 core) is assumed to be constant, changes in slope are assumed to be due to changes in sedimentation rate within the *test* core. One may correct for these presumed changes in sedimentation rate by transforming depths in the test core to depths in the reference core.

In their analysis, Prell et al. (1986) combined the RC11–120 and E49–18 $\delta^{18}\text{O}$ data into a single isotopic signal *before* comparing this composite signal to the V28–238 reference signal. However, this is *extremely* dubious, because their new depth scale had to be, to some degree, fictitious. This is because one particular isotopic feature, the MIS 6–5 boundary (or, in decimal notation, MIS Event 6.0), was located at one depth (440 cm) within the RC11–120 and at another depth (490 cm) in the E49–18 cores. Which depth, then, was plotted on the Shaw diagram? Based on their Figure 6, it appears that Prell et al. (1986, p. 151) used the RC11–120 depth scale. This means that depths within the E49–18 core had to somehow be converted to the RC11–120 depth scale before they constructed their Shaw diagram. But this would require them to make *assumptions* about the relative sedimentation rates for the RC11–120 and E49–18 cores. But the very purpose of a Shaw diagram is to *check* for changes in sedimentation rates, rather than to simply make assumptions about those rates! Would it not make more sense to actually *check* for relative changes in sedimentation rates in the two cores *separately*? Then, *after* such changes had been identified and corrected *separately* in both cores, the two data sets could be combined into a composite data set, if need be, on a common depth scale.

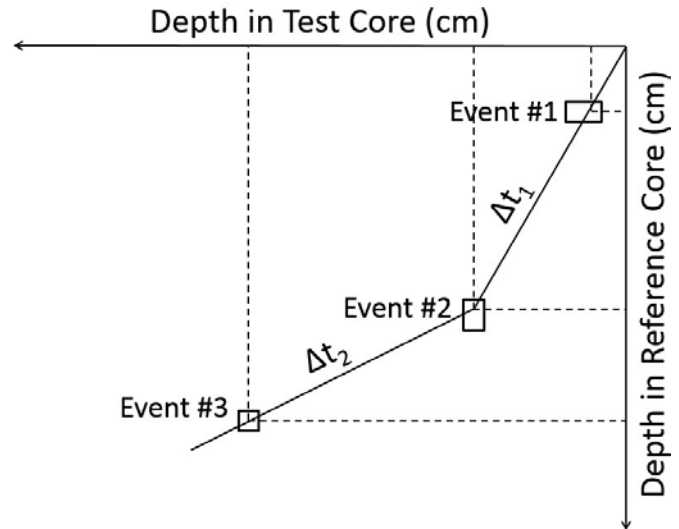


Figure 6. Conceptual illustration of a Shaw diagram, which compares the sedimentation rates within a test core to the (presumably constant) sedimentation rate in a “standard” core, such as V28–238. Each small box illustrates the depth uncertainties for a given isotopic event that has been identified in both the test and standard cores.

For this reason, I constructed *separate* Shaw diagrams for the RC11–120 and E49–18 cores. With a few exceptions, I used the isotopic features identified by Prell et al. (1986) and Howard and Prell (1992). However, because I used a newer version of the RC11–120 $\delta^{18}\text{O}$ data than did Howard and Prell (1992), my estimates for the locations of some isotopic events differed from theirs, particularly near the bottom of the RC11–120 core.

Isotopic Events Used in the Analysis

The isotopic events identified by Howard and Prell (1992) within the RC11–120 and E49–18 cores are listed in their Table 3 (pp. 88–90). Likewise, the depth range (maximum and minimum possible depths) associated with each isotopic event within the V28–238 core are found within Table 2 (pp. 144–148) in Prell et al. (1986). Note that the notation “SRC” in Prell et al.’s Table 2 refers to the V28–238 core (Prell et al., 1986, p. 148). Actually, “SRC” seems to be a typo; Prell et al. called V28–238 the standard reference *section* (p. 148); hence the acronym at the head of their Table 2 should really be “SRS,” as it is in their Figure 1 caption. The most likely position of each V28–238 isotopic event was obtained by visual inspection of a graph of the V28–238 $\delta^{18}\text{O}$ data, plotted as a function of depth. These data were obtained from <https://>

Table 2. Marine isotope stage events in the RC11–120 deep-sea core that were used to place the RC11–120 data on the V28–238 depth/age scales.

MIS Event	RC11–120 Min. Depth (cm)	RC11–120 Most Likely Depth (cm)	RC11–120 Max Depth (cm)
1.1	10	20	30
2.0	30	45	55
2.2	60	70	85
3.3	175	185	195
4.0	205	215	220
4.2	220	225	235
5.0	245	250	270
5.1	255	290	300
5.5	410	420	435
6.0	435	440	455
6.6	595	600	605
7.0	605	620	635
7.1	630	645	655
7.3	670	675	695
7.4	700	722.5	740
7.5	740	760	775
8.0	775	785	790
8.2	790	805	820
8.3	815	830	840
8.4	835	840	855
8.5	855	865	895
8.6	865	895	905
9.0	900	910	920
9.1	920	927.5	940
9.2	940	950	950

doi.pangaea.de/10.1594/PANGAEA.51710?format=html#download . Generally, there was very good agreement between the depth ranges listed by Prell et al. (1986) and the online V28–238 $\delta^{18}\text{O}$ data.

Prell et al. (1986) further narrowed the possible depth ranges of MIS events by comparing data from more than a dozen sediment cores. They also listed these more restrictive

depth ranges in their Table 2. However, I elected not to use these narrower depth ranges to construct my Shaw diagrams for a number of reasons. First, Prell et al. (1986) also used the RC11–120 and E49–18 data to obtain these narrower depth ranges. However, as noted earlier, they incorrectly “lumped” the RC11–120 and E49–18 data together (their p. 151), treating them as data obtained from a single core. Hence, this error could have biased their results. Attempting to correct for their mistake would require making separate Shaw diagrams for *all* the dozen or so sediment cores used in Prell et al.’s (1986) study, and then attempting to find an overall error range for each MIS event. Needless to say, this would be a *lot* of work, and it does not seem necessary; although the incorrect “lumping” of the RC11–120 and E49–18 data together may have biased the results somewhat, the Shaw diagrams one obtains using the narrower error ranges (their so-called SCU values) are very similar to those obtained otherwise (the SRC values from the V28–238 core). Hence, using the wider error ranges for the MIS events is unlikely to significantly alter the overall results, and given the effort required to obtain those narrower error ranges, it is likely not worth the effort. Second, it seems reasonable to avoid using data from a large number of cores, since doing so requires correct identification of the same (presumably global) MIS events in *all* the dozen or so cores. This greatly increases the possibility of incorrect identification of an MIS event or events.

Obtaining the RC11–120 Line of Correlation

The twenty-five isotopic features I used to place the RC11–120 data on the V28–238 depth scale are shown in Table 2. Most of these features came from the list provided by Howard and Prell (1992). However, none of their identified isotopic features were located within the uppermost 100 cm or so of the RC11–120 core. In order to obtain a better “spread” of data close to the origin, I also included the 1.1, 2.0, and 2.2 MIS features. These isotopic events seemed like reasonable additions to the list since they are fairly easy to identify. I also included the 8.6, 9.0, 9.1, and 9.2 MIS events. These four events were not included in Howard and Prell’s list, but I included them to reduce uncertainty in the new depth scale at the bottom of the core. This was rather tricky, due to a gap of missing $\delta^{18}\text{O}$ data between 865 and 895 cm, but I estimated the locations of these four events to the best of my ability by assuming that the prominent $\delta^{18}\text{O}$ peak at 895 cm was MIS Event 8.6, and that the very bottom of the core (depth of 950 cm) was MIS Event 9.2. Note that this caused my depth assignments for MIS Events 8.4 and 8.5 to be noticeably different from the depths assigned by Howard and Prell. However, this seemed on balance to be more charitable to the Milankovitch theory, as my depth assignments were more consistent with those implied by Hays, Imbrie, and

Shackleton’s (1976) Figure 2, and those assignments yielded results that were quite favorable to the theory.

I estimated the minimum and maximum possible depths for each RC11–120 isotopic features to the best of my ability, although this eventually turned out to be unnecessary. As a general rule, the “line of correlation” does not necessarily have to pass through the “centers” of all the data points; it only needs to fall within each of the error “boxes” for each point. Obviously, one needs to know the estimated errors in order to meet this requirement. However, I discovered through trial and error that better alignment results between the corresponding $\delta^{18}\text{O}$ troughs and peaks of the test and reference cores if one *does* force the line of correlation to pass through the “centers” of all the data points. This makes sense, because the “center” of each data point represents the “most likely” location of the corresponding isotopic event. Figure 7 shows the Shaw diagram for the RC11–120 and V28–238 $\delta^{18}\text{O}$ data, and Figure 8 shows the RC11–120 and V28–238 $\delta^{18}\text{O}$ data, both plotted on the V28–238 depth scale. There is very good alignment between the corresponding $\delta^{18}\text{O}$ features within the two cores, showing that the RC11–120 data has been successfully placed on the V28–238 depth scale.

Obtaining the E49–18 Line of Correlation

In a similar fashion, I plotted 25 isotopic events common to both the E49–18 and V28–238 cores (Figure 9). All but three of these isotopic events were included in Howard and Prell’s (1992) E49–18 data from their Table 3. Their table excluded the MIS 6–5 and 8–7, and 12–11 stage boundaries (the MIS 6.0, 8.0, and 12.0 events), but it seemed reasonable to include them since these were age anchor points used in the Pacemaker

analysis. Figures 3 and 4 show the locations of the identified isotopic events in the two cores, and Tables 1 and 3 provide these data in tabular form. Occasionally, the discrete nature of the data required me to place an event between two data points; for instance, the isotopic event 6.0 in E49–18 should be about halfway between the data points at 490 cm and 500 cm; hence, I reported this depth as 495 cm.

I chose to exclude from my analysis data from above MIS event 6.0 in the E49–18 core, as did the Pacemaker authors, mainly because use of those data points would have added

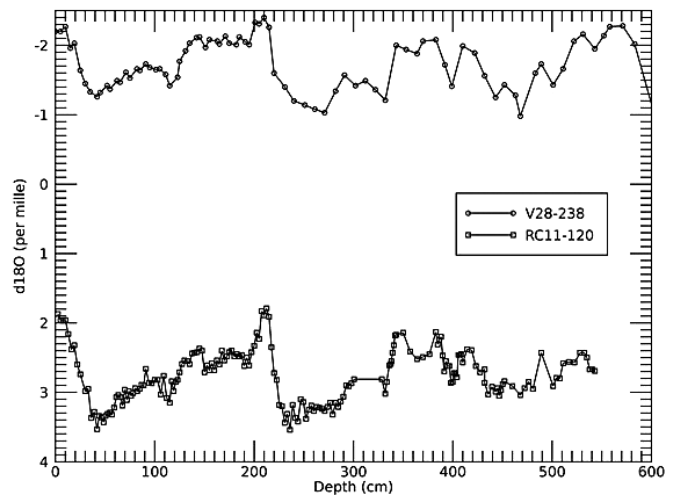


Figure 8. Comparison of the RC11–120 and V28–238 $\delta^{18}\text{O}$ signals, after the RC11–120 data were placed on the revised V28–238 depth scale.

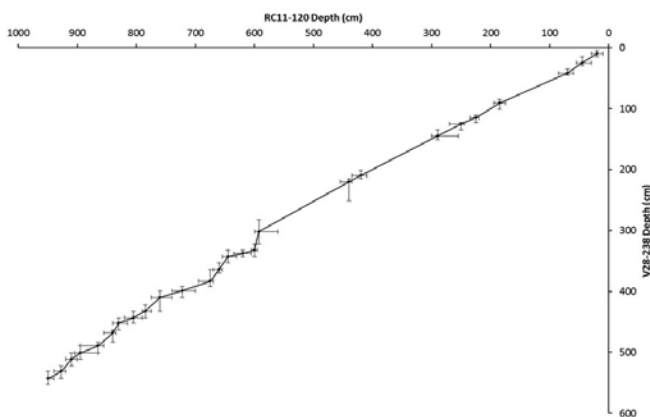


Figure 7. My Shaw diagram for the RC11–120 and V28–238 $\delta^{18}\text{O}$ data, constructed using the MIS events common to Tables 1 and 2.

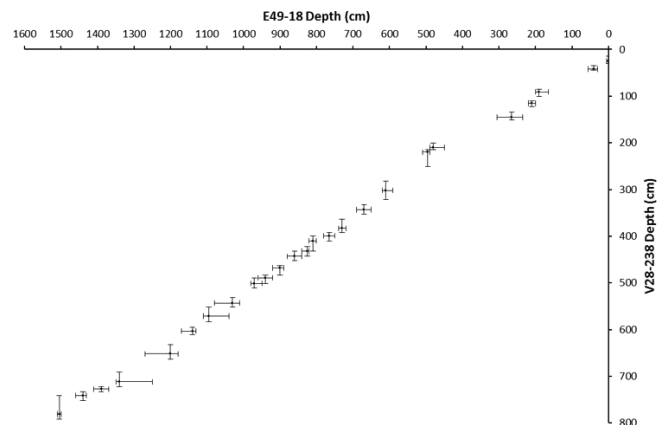


Figure 9. MIS events identified in both the E49–18 and V28–238 $\delta^{18}\text{O}$ data.

Table 3. Marine isotope stage events in the E49–18 deep-sea core that were used to place the E49–18 data on the V28–238 depth/age scales, as well as the six MIS events in the uppermost core section that were not used in this analysis.

MIS Event	E49–18 Min. Depth (cm)	E49–18 Most Likely Depth (cm)	E49–18 Max Depth (cm)
2.0	0	0	5
2.2	30	40	55
3.3	165	190	200
4.2	200	210	220
5.1	235	265	305
5.5	450	480	490
6.0	490	495	510
6.5	590	610	620
7.1	650	670	690
7.3	720	730	740
7.4	750	765	780
7.5	800	810	820
8.0	820	825	840
8.2	840	860	880
8.4	890	900	920
8.5	920	940	960
8.6	950	970	980
9.2	1010	1030	1080
9.3	1040	1095	1110
10.2	1130	1140	1170
11.1	1180	1200	1270
11.3	1250	1340	1350
12.0	1370	1390	1410
12.2	1430	1440	1460
13.0	1500	1505	1510

six additional line segments to my line of correlation (LOC). Even without using data from the top of the core, I still needed eighteen linear equations to place the E49–18 data on the V28–238 depth scale. And since the Pacemaker authors did not use the data from the uppermost part of the core, why should I have to, especially when doing so requires five additional

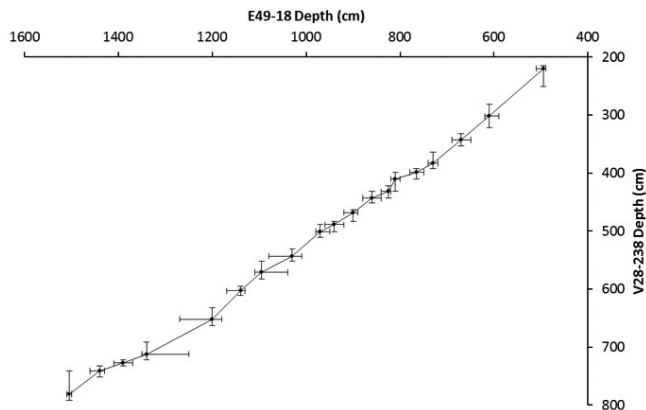


Figure 10. My Shaw diagram for the E49–18 $\delta^{18}O$ data (bottom two-thirds only) and the V28–238 data, constructed using the MIS events common to Tables 1 and 3.

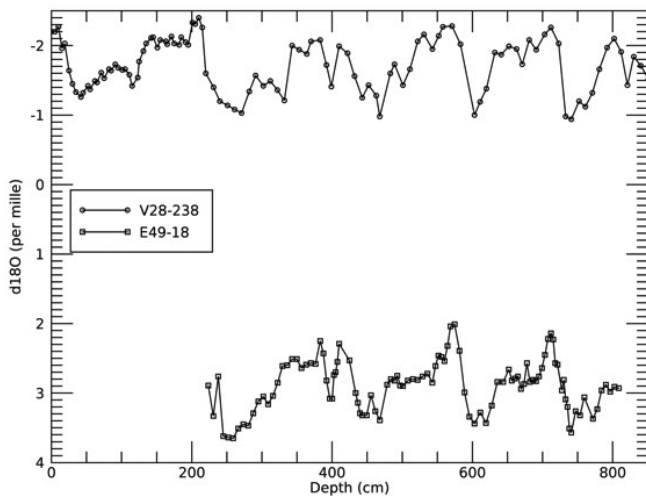


Figure 11. Comparison of the E49–18 and V28–238 $\delta^{18}O$ signals, after the E49–18 data were placed on the revised V28–238 depth scale.

linear equations? Figure 10 shows the Shaw diagram that was used to place the lower two-thirds of E49–18 data onto the V28–238 depth scale.

The E49–18 $\delta^{18}O$ data are shown in Figure 11, along with the V28–238 data, after placing the E49–18 data on the V28–238 depth scale. Note that the alignment between

corresponding isotopic features is pretty good but not as good as the alignment between the RC11–120 and E49–18 $\delta^{18}\text{O}$ features. One could improve this alignment by using additional MIS events in the Shaw diagram, but one runs the risk of misidentifying some of the additional isotopic features. Note also that the “spike” in the E49–18 $\delta^{18}\text{O}$ signal at about 240 cm in Figure 11 is not a mistake, even though it does not align with a comparable $\delta^{18}\text{O}$ feature in the V28–238 data; this feature is simply not present in the V28–238 $\delta^{18}\text{O}$ data.

After placing the RC11–120 and E49–18 data onto the V28–238 depth scale, I used the equation

$$\text{Age (ka)} = \frac{\text{depth (cm)}}{1170 \text{ cm}} \times 780 \text{ ka} \quad (2)$$

to transform the V28–238 depth scale into a timescale.

New Results

The original Pacemaker paper results were seen as strong evidence for Milankovitch climate forcing because the apparent lengths of the climate cycles (100, 42, and 23 ka) within the geological spectra were very close to those of calculated astronomical cycles (100, 41, and 23 ka). Of course, the revisions uniformitarian scientists themselves have made to the sediment core data have undone those original results. After making these revisions, but still using the methodologies of Shackleton and Opdyke (1973) and Hays, Imbrie, and Shackleton (1976), I redid the Pacemaker power spectrum calculations, the results of which are shown in Figures 12–20. The use of newer $\delta^{18}\text{O}$ data sets sometimes moved slightly the locations of the age control points used by the Pacemaker authors; the MIS 6.0 and 12.0 events in the E49–18 core are now located at 495 cm and 1390 cm, respectively, rather than 490 cm and 1405 cm, as originally reported in the Pacemaker paper.

Dashed double arrows within the figures indicate the approximate bandwidth for each spectrum, the meaning of which is discussed in Hebert (2016b, p. 138). In the Pacemaker paper, the original timescales for the RC11–120 and E49–18 cores were arguably too short to obtain a good estimate of the period of the eccentricity cycle, and the Pacemaker authors did not bother doing so. However, the newer timescales (358 ka for the RC11–120 core and 390 ka for the E49–18 core section) are long enough to attempt to obtain these estimates, so I did so.

Vertical lines in each figure indicate the frequencies/periods of the eccentricity, obliquity, and precession orbital cycles for the calculated time intervals. In some cases, a resulting astronomical peak was quite short relative to the other peaks, or there was considerable uncertainty in the estimate of the

eccentricity frequency/period, as the eccentricity period was a large fraction of the time interval assigned to the core. In those cases, the vertical lines are dashed to indicate greater uncertainty in those astronomical frequencies/periods.

The new RC11–120 timescale extends from 0 ka to 362 ka. Because some of the RC11–120 data are missing from the very top of the core, I elected to set (after interpolation of the data) the timescale from 4 to 362 ka, so that all three data sets would “cover” the same time interval. I used an interpolated time-step $\Delta t = 2$ ka, which resulted in $n = 180$ interpolated data points. The power spectra in Figures 13 through 15 were obtained with the variable m set to 110 (see Hebert 2016b, pp. 135–138, for a discussion of the meaning of this parameter). Spectral analysis performed on the orbital variables over this same time interval (and using the same values of m and n) were used to obtain the expected Milankovitch periods/frequencies. I used Berger and Loutre’s (1991) orbital data, accessed at <https://doi.pangaea.de/10.1594/PANGAEA.56040?format=html#lcol0.ds1004521>.

Before examining Figures 12–20, how do we determine if the (central) frequency f_0 of a climate peak agrees with the frequency obtained from the Milankovitch theory? As a first approximation, one can take the uncertainty in the (central) frequency f_0 of a spectral peak to be half the width of the peak, measured at half the peak’s full height. In other words, the uncertainty in the frequency is the half-width at half maxima (HWHM). Hence, if a theoretically expected orbital frequency lies inside the full-width-at-half maxima (FWHM) of the spectral climate peak, then one can consider the central frequency f_0 of the climate peak to agree with the frequency of the astronomical peak (Muller and MacDonald, 2000, pp. 96–98).

Of course, there is also uncertainty in the orbital frequencies, so one might wonder if perhaps we should calculate error bars for the orbital spectra, too, and then check to see if the climate and orbital error bars overlap. However, this is not necessary. The uncertainty in a spectral frequency is mainly due the background noise (Muller and MacDonald, 2000, p. 96). Thus, the greater the height of a spectral peak compared to the background spectral power, the less the uncertainty in the estimate of the frequency (Muller and MacDonald, 2000, p. 98). Orbital spectra have extremely high signal-to-background ratios, so we can treat the uncertainties in the orbital frequencies as being negligible.

The RC11–120 SST results (Figure 12) are not particularly impressive. The expected precession frequencies do fall within the full-width-at-half-maxima (FWHM) for the F and G “peaks,” although it is debatable whether these short “bumps” can really be called “peaks.” The obliquity frequency just barely falls outside the FWHM of the C peak. However, the A peak is arguably consistent with Milankovitch expectations, as the second eccentricity frequency does fall within the FWHM of the A peak.

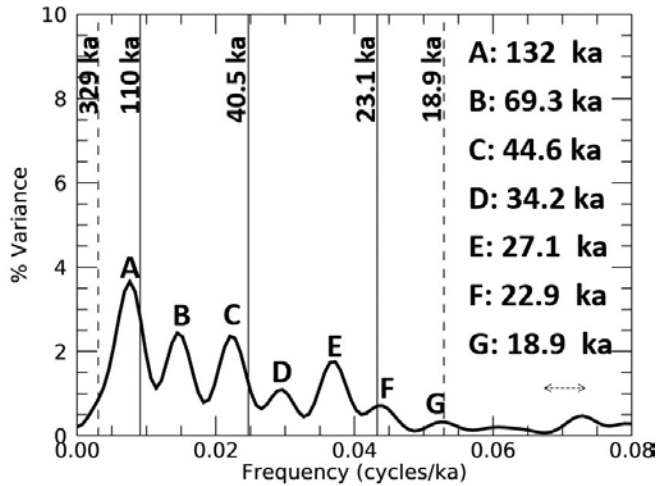


Figure 12. Revised RC11–120 SST power spectrum.

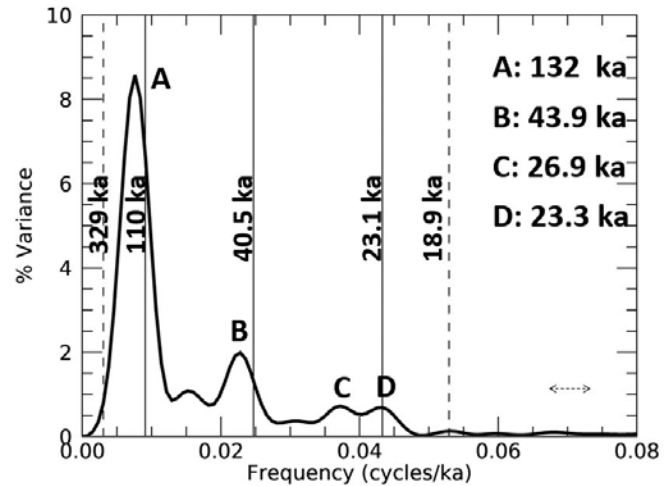


Figure 13. Revised RC11–120 $\delta^{18}\text{O}$ power spectrum.

The RC11–120 $\delta^{18}\text{O}$ spectral results (Figure 13) are in better agreement with Milankovitch expectations. The lower precession frequency (corresponding to 23.1 ka) falls within the FWHM of the D peak. However, no climate peak appears at the higher precession frequency (corresponding to 18.9 ka), but given the uncertainty and relatively low height of this precession peak, this may not be a problem. The obliquity frequency just falls on the rightmost edge of the FWHM for the B peak. The A peak is in agreement with the eccentricity frequency.

The RC11–120 % *C. davisiana* spectral results (Figure 14) are in considerably worse agreement with Milankovitch expectations. The A peak, according to the FWHM rule, is barely in agreement with Milankovitch expectations, but this is not the case for the B or C peaks.

The spectral results for data from the bottom two-thirds of the E49–18 core are in extremely poor agreement with Milankovitch expectations, as can be seen from Figures 15–17. After interpolation of the original data, the timescale extended from 149 to 539 ka ($n = 131$ data points, with $\Delta t = 3.0$ ka). The parameter m was set equal to 80. Again, the timescale of 539 ka – 149 ka = 390 ka is arguably long enough to calculate a theoretical value for the eccentricity frequency/period, so I did so. However, the width of this eccentricity peak was quite wide, so I used a dashed vertical line to indicate greater uncertainty in this particular frequency value. A “doublet” was again present in the precession power spectrum.

Given these equivocal results, construction of the PATCH composite data sets is not really justified, but for the sake of completeness I constructed them anyway. The new PATCH timescale (after interpolation) extended from 4 to 539 ka

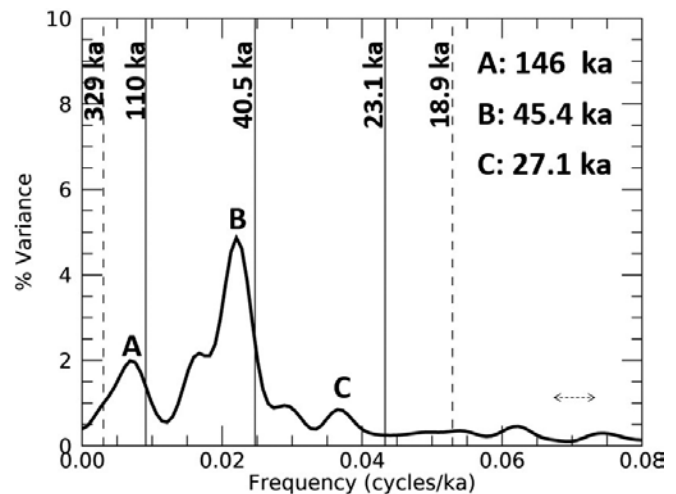


Figure 14. Revised RC11–120 % *C. davisiana* power spectrum.

(again, because some data were missing from the uppermost part of the RC11–120 core; the age scale was started at 4 ka). Because the radiocarbon age assignment of 9.4 (± 0.6) ka at a depth of 39 cm within the RC11–120 core contradicted the age assignment of 14.3 ka inferred from Eq. 2, this particular age control point was excluded from the analysis. Interpolation resulted in $n = 215$ data points with $\Delta t = 2.5$ ka. The parameter m was set equal to 95. Because a test of statistical significance implicitly assumes that the data are weakly stationary (Hu,

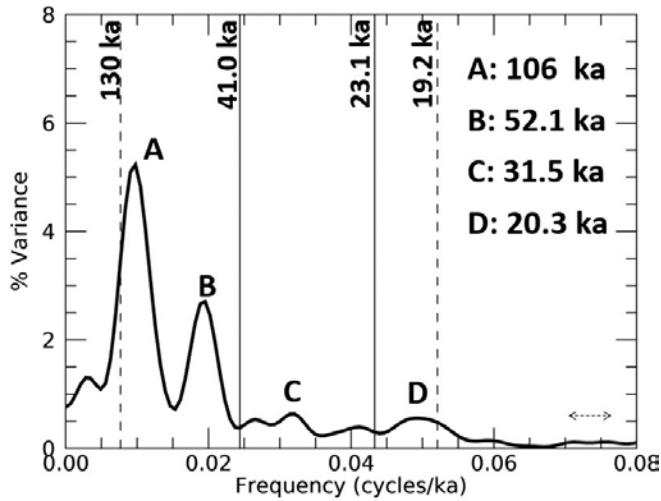


Figure 15. Revised E49-18 SST power spectrum.

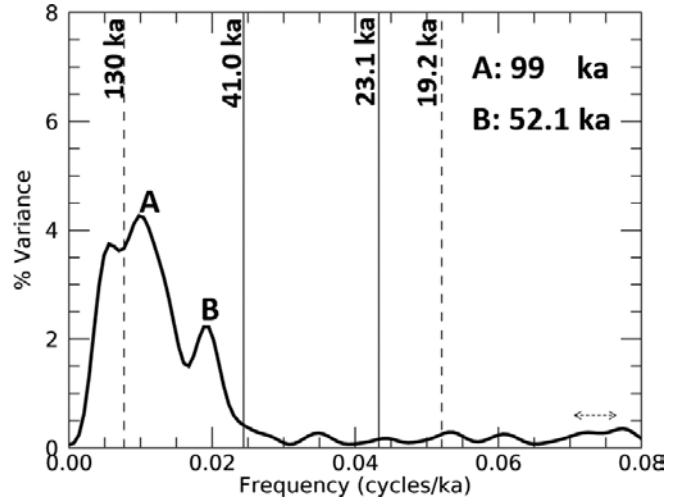


Figure 17. Revised E49-18 % *C. davisiana* power spectrum.

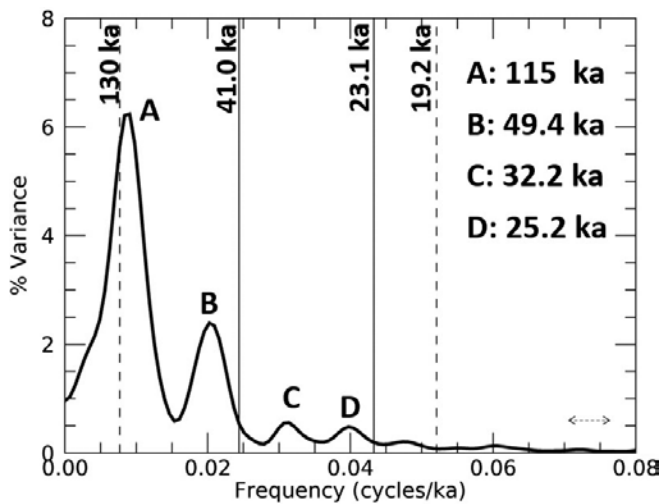


Figure 16. Revised E49-18 $\delta^{18}\text{O}$ power spectrum.

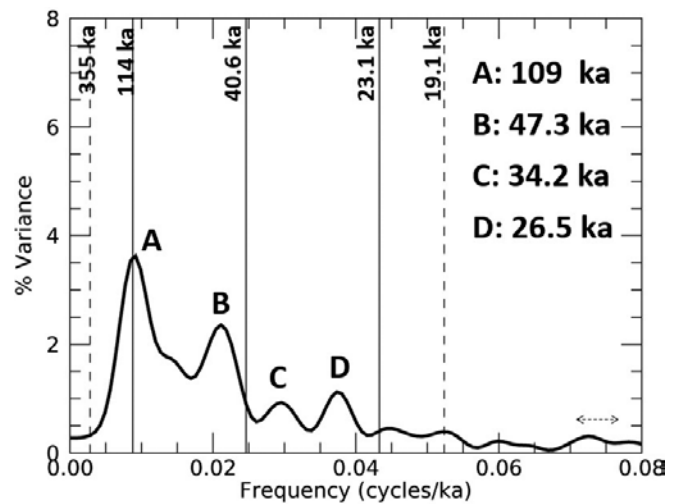


Figure 18. Revised PATCH SST power spectrum.

2006), I de-trended the RC11-120 and E49-18 data separately and normalized their standard deviations to 1.0 before combining them into a single data set (Hebert, 2016c, p. 245). Again, there was poor agreement between Milankovitch expectations and the actual results.

Some uniformitarian scientists claim that the age of the Brunhes-Matuyama magnetic reversal boundary is actually 790 ka (Berger et al., 1995; Karner et al., 2002; Muller and MacDonald 2000, p. 159). I used the lower age estimate of 780

ka in order to be charitable to the Milankovitch hypothesis. Using the higher age estimate will “stretch” the timescales for the sediment cores even further, potentially yielding results that are in even poorer agreement with the Milankovitch hypothesis!

Conclusion

Although Hebert (2016c) already demonstrated that the revision to the age of the Brunhes-Matuyama magnetic reversal

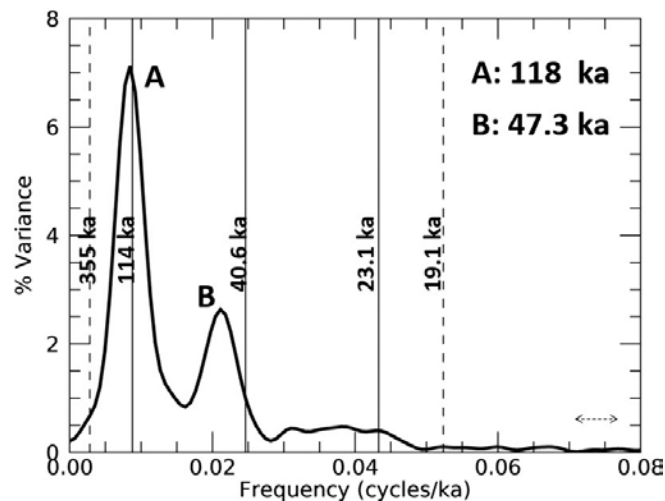


Figure 19. Revised PATCH $\delta^{18}\text{O}$ power spectrum.

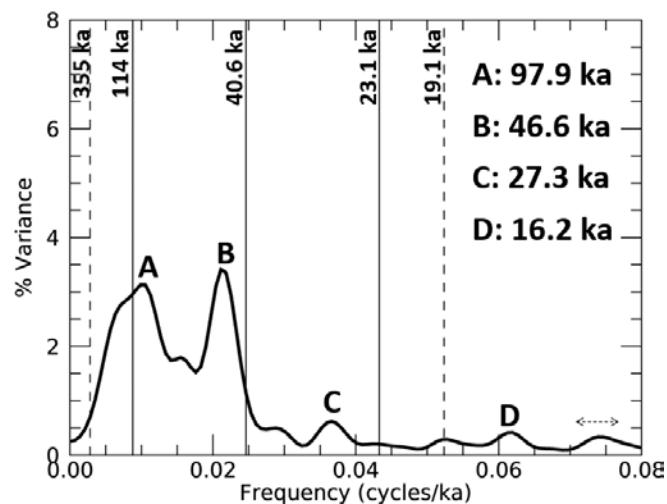


Figure 20. Revised PATCH % *C. davisiana* power spectrum.

boundary adversely affected the original Pacemaker results, there remained a slim but nonzero chance that these additional changes could collectively “cancel” each other out, yielding results that were again consistent with Milankovitch expectations. The results of this paper seem to have closed that potential loophole. Of course, uniformitarian scientists might “quibble” with these results on the grounds that they do not like my choice of MIS events that I used to construct my Shaw diagrams. Admittedly, this was the hardest part of this research

project. The selection of the MIS events involved “judgment calls,” and in some cases, it was genuinely difficult deciding whether or not an MIS event should be included in the Shaw diagrams, especially if that event was not included in the lists by Prell et al. (1986) and Howard and Prell (1992). However, I don’t think “tinkering” with the choice of MIS events is likely to affect the results that much. I have done multiple trials using different combinations of MIS events, and none of them provided convincing evidence of the Milankovitch theory. If uniformitarian climatologists want to contest these results, they are certainly welcome to do the calculations for themselves, something that, candidly, they should have done more than 25 years ago!

It is obvious that the “Pacemaker” results cannot legitimately be used as an argument for Milankovitch climate forcing—even if uniformitarian paleoclimatologists are unwilling to publicly admit this!

References

- Berger, A., and M.F. Loutre. 1991. Insolation values for the climate of the last 10 million years. *Quaternary Science Reviews* 10(4): 297–317.
- Berger, W.H., T. Bickert, G. Wefer, and M.K. Yasuda. 1995. Brunhes-Matuyama boundary: 790 k.y. date consistent with ODP Leg 130 oxygen isotope records based on fit to Milankovitch template. *Geophysical Research Letters* 22, no. 12 (June 15): 1525–1528.
- Bogue, S.W., and J.M.G. Glen. 2010. Very rapid geomagnetic field change recorded by the partial remagnetization of a lava flow. *Geophysical Research Letters* 37, L21308.
- Clement, B.M. 2004. Dependence of the duration of geomagnetic polarity reversals on site latitude. *Nature* 428:637–640.
- Coe, R.S., M. Prévot, and P. Camps. 1995. New evidence for extraordinarily rapid change of the geomagnetic field during a reversal. *Nature* 374:687–692.
- Cronin, T.M. 2010. *Paleoclimates: Understanding Climate Change Past and Present*. Columbia University Press, New York, NY.
- Emiliani, C., and N.J. Shackleton. 1974. The Brunhes Epoch: isotopic paleotemperatures and geochronology. *Science* 183, no. 4124 (February 8): 511–514.
- Gibbard, P.L. 2007. Climatostratigraphy. In Elias, S.A. (editor), *Encyclopedia of Quaternary Science*, pp. 2819–2825. Elsevier, Amsterdam, The Netherlands. Quoted in modified form by the INQUA Commission on Stratigraphy and Chronology, <http://www.inqua-saccomm.org/stratigraphic-guide/climatostratigraphy-geological-climate-stratigraphy/> (accessed April 23, 2015).
- Hays, J.D. 1997. Sea surface temperature reconstruction from sediment core RC11–120 (specmap.051). doi: 10.1594/PAN-GAEA.52223.
- Hays, J.D., J. Imbrie, and N.J. Shackleton. 1976. Variations in the

- earth's orbit: pacemaker of the ice ages. *Science* 194(4270): 1121–1132.
- Hays, J.D., J.D. Imbrie, and N.J. Shackleton. 1997. Stable isotopes of sediment core ELT49.018-PC (specmap2.006). doi:10.1594/PANGAEA.52207.
- Hebert, J. 2016a. Revisiting an iconic argument for Milankovitch climate forcing: should the “Pacemaker of the Ice Ages” paper be retracted? Part 1. *Answers Research Journal* 9:25–56.
- Hebert, J. 2016b. Revisiting an iconic argument for Milankovitch climate forcing: should the “Pacemaker of the Ice Ages” paper be retracted? Part 2. *Answers Research Journal* 9:131–147.
- Hebert, J. 2016c. Revisiting an iconic argument for Milankovitch climate forcing: should the “Pacemaker of the Ice Ages” paper be retracted? Part 3. *Answers Research Journal* 9:229–255.
- Hebert, J. 2017a. A broken climate pacemaker? Part 1. *Journal of Creation* 31(1): 88–98.
- Hebert, J. 2017b. A broken climate pacemaker? Part 2. *Journal of Creation* 31(1): 104–110.
- Hebert, J. 2017c. Testing old-earth climate claims, part 1. *Acts & Facts* 46(11): 10–13.
- Hebert, J. 2017d. Testing old-earth climate claims, part 2. *Acts & Facts* 46 (12): 10–13.
- Hilgen, F.J. 1991. Astronomical calibration of Gauss to Matuyama sapropels in the Mediterranean and implication for the geomagnetic polarity time scale. *Earth and Planetary Science Letters* 104(2–4): 226–244.
- Hodell, D.A. 2016. The smoking gun of the ice ages. *Science* 354(6317): 1235–1236.
- Howard, W.R., and W.L. Prell. 1992. Late Quaternary surface circulation of the southern Indian Ocean and its relationship to orbital variations. *Paleoceanography* 7, 1 (February): 79–117.
- Hu, L. 2006. Lecture 1: Stationary time series. Lecture notes for Ohio State University economics class. <http://www.econ.ohio-state.edu/dejong/notel.pdf>.
- Humphreys, D.R. 1986. Reversals of the earth's magnetic field during the Genesis Flood. In Walsh, R.E., C.L. Brooks, and R.S. Crowell (editors), *Proceedings of the First International Conference on Creationism*, pp. 113–123. Creation Science Fellowship, Pittsburgh, PA.
- Humphreys, D.R. 1990. Physical mechanism for reversals of the earth's geomagnetic field during the Flood. In Walsh, R.E., and C. L. Brooks (editors), *Proceedings of the Second International Conference on Creationism, Technical Symposium Sessions*, pp. 129–140. Creation Science Fellowship, Pittsburgh, PA.
- Imbrie, J., J.D. Hays, D.G. Martinson, A. McIntyre, A.C. Mix, J. Morley, N.G. Pisias, W.L. Prell, and N.J. Shackleton. 1984. The orbital theory of Pleistocene climate: support from a revised chronology of the marine $\delta^{18}\text{O}$ record. In Berger, A., J. Imbrie, J. Hays, G. Kukla, and B. Saltzman (editors), *Milankovitch and Climate, Part 1*, pp. 269–305. D. Reidel Publishing, Dordrecht, The Netherlands.
- Karner, D.B., J. Levine, B.P. Medeiros, and R.A. Muller. 2002. Constructing a stacked benthic $\delta^{18}\text{O}$ record. *Paleoceanography* 17, no. 3 (September): 2–1–2–16.
- Kingston, P.F. 2010. Benthic organisms overview. In Steele, J.H. (editor), *Climates and Oceans*, pp. 416–424. Academic Press, Amsterdam, The Netherlands.
- Martinson, D.G., N.G. Pisias, J.D. Hays, J.D. Imbrie, T.C. Moore, and N.J. Shackleton. 1987. Stable isotopes and sea surface temperatures reconstructed from sediment core RC11–120. Appendix in Martinson, D.G., N.G. Pisias, J.D. Hays, J.D. Imbrie, T.C. Moore, and N.J. Shackleton. Age dating and the orbital theory of the ice ages: development of a high-resolution 0 to 300,000-year chronostratigraphy. *Quaternary Research* 27:1–29.
- Maslin, M. 2016. Forty years of linking orbits to ice ages. *Nature*. 540 (7632): 208–210.
- McIntyre, A., and J.D. Imbrie. 2000. Stable Isotope of Sediment Core RC11–120 (specmap.013). doi:10.1594/PANGAEA.56357.
- McManus, J.F., G.C. Bond, W.S. Broecker, S. Johnsen, L. Labeyrie, and S. Higgins. 1994. High-resolution climate records from the North Atlantic during the last interglacial. *Nature* 371 (September 22): 326–329.
- Mortyn, P.G., and C.D. Charles. 2003. Planktonic foraminiferal depth habitat and $\delta^{18}\text{O}$ calibrations: plankton tow results from the Atlantic sector of the Southern Ocean. *Paleoceanography* 18(2): 1037.
- Muller, R.A., and G.J. MacDonald. 2000. *Ice Ages and Astronomical Causes: Data, Spectral Analysis and Mechanisms*. Praxis Publishing, Chichester, UK.
- Oard, M.J. 1984. Ice ages: the mystery solved? Part II: the manipulation of deep-sea cores. *Creation Research Society Quarterly* 21:125–137.
- Oard, M.J. 2005. The astronomical theory of the Ice Age becomes more complicated. *Journal of Creation* 19(2): 16–18.
- Oard, M.J. 2007. Astronomical troubles for the astronomical hypothesis of ice ages. *Journal of Creation* 21(3): 19–23.
- Oard, M.J. 2014. Phase problems with the astronomical theory. *Journal of Creation* 28(2): 11–13.
- Prell, W.L., J. Imbrie, D.G. Martinson, J.J. Morley, N.G. Pisias, N.J. Shackleton, and H.F. Streeter. 1986. Graphic correlation of oxygen isotope stratigraphy application to the Late Quaternary. *Paleoceanography* 1, no. 2 (June): 137–162.
- Rickaby, R.E.M., and H. Elderfield. 1999. Planktonic foraminiferal Cd/Ca: paleonutrients or paleotemperature? *Paleoceanography* 14(3): 293. ftp://ftp.ncdc.noaa.gov/pub/data/paleo/paleocean/sediment_files/complete/e49-18r-tab.txt (accessed May 25, 2017).
- Sagnotti, L., G. Scardia, B. Giaccio, J.C. Liddicoat, S. Nomade, P.R. Renne, and C.J. Sprain. 2014. Extremely rapid directional change during Matuyama-Brunhes geomagnetic polarity reversal. *Geophysics Journal International* 199, no. 2 (November): 1110–1124.
- Shackleton, N.J. and N.D. Opdyke. 1973. Oxygen isotope and palaeo-geomagnetic stratigraphy of equatorial Pacific core V28–238: oxygen

- isotope temperatures and ice volumes on a 10^5 year and 10^6 year scale. *Quaternary Research* 3:39–55.
- Shackleton, N.J., A. Berger, and W.R. Peltier. 1990. An alternative astronomical calibration of the Lower Pleistocene timescale based on ODP site 677. *Transactions of the Royal Society of Edinburgh: Earth Sciences* 81, no. 4 (January): 251–261.
- Shaw, A.B. 1964. *Time in Stratigraphy*. McGraw-Hill, New York, NY.
- Spell, T.L., and I. McDougall. 1992. Revisions to the age of the Brunhes-Matuyama boundary and the Pleistocene geomagnetic polarity timescale. *Geophysical Research Letters* 19(12): 1181–1184.
- Vardiman, L. 1997. Rapid changes in oxygen isotope content of ice cores caused by fractionation and trajectory dispersion near the edge of an ice shelf. *Journal of Creation* (formerly *Creation Ex Nihilo*) 11 (part 1): 52–60.
- Walker, M., and J. Lowe. 2007. Quaternary science 2007: a 50-year retrospective. *Journal of the Geological Society, London* 164:1073–1092.
- Woodward, J. 2014. *The Ice Age: A Very Short Introduction*. Oxford University Press, Oxford, UK.
- Wright, J.D. 2010. Cenozoic climate—oxygen isotope evidence. In Steele, J.H. (editor), *Climates and Oceans*, pp. 316–327. Academic Press, Amsterdam, The Netherlands.